Spectral redshift versus broadening from photon and dilepton spectra

Jan-e Alam,[1,3] Pradip Roy,[2] Sourav Sarkar,[3] and Bikash Sinha[2,3]
[1]*Physics Department, University of Tokyo, Tokyo 113-0033, Japan*
[2]*Saha Institute of Nuclear Physics, 1/AF Bidhannagar, Kolkata 700 064, India*
[3]*Variable Energy Cyclotron Centre, 1/AF Bidhannagar, Kolkata 700 064, India*
(Received 2 January 2003; published 7 May 2003)

We estimate the photon and dilepton emission rates from hot hadronic matter with in-medium spectral shift and broadening of vector mesons. It is observed that both the WA98 photon data and CERES/NA45 dilepton data can be well reproduced with similar initial conditions. The freeze-out condition has been constrained by the transverse mass spectra of pions and protons measured by the NA49 Collaboration. We argue that simultaneous measurement of the p_T spectra of single photons as well as invariant mass distribution of dileptons is crucial to understand the in-medium spectral function of the vector mesons.

DOI: 10.1103/PhysRevC.67.054901 PACS number(s): 25.75.−q, 12.40.Vv, 13.85.Qk, 21.65.+f

I. INTRODUCTION

The study of the behavior of hadrons at finite temperature and/or high baryon density has attracted substantial theoretical and experimental attention in recent times. The theoretical motivation stems from the expectation that broken chiral symmetry of QCD might be restored at high temperature and/or density, at least partially, and this has nontrivial effects on the spectra of low lying hadronic states. Again, these studies are of considerable importance in connection with the experimental detection and study of quark gluon plasma (QGP) in the ultrarelativistic collisions of heavy ions. This is because disentangling the signals from quark matter would require a precise estimate of emissions from hadronic sources, which constitutes an overwhelming background in such experiments. Now, the properties of short-lived resonances such as the ρ and ω mesons which are likely to decay within the fireball can only be studied through deep probes such as photons and lepton pairs which are essentially electromagnetically interacting and thus probe the entire space-time volume of the collision [1]. The medium modifications of low mass vector mesons has been the subject of numerous theoretical investigations culminating broadly into the following two types of predictions. QCD based models predict a downward shift in the mass, which we will mention as spectral redshift, and a rescattering scenario giving rise to an enhanced width, which we have denoted by spectral broadening, the mass remaining largely unchanged. Our aim in this work is to calculate the electromagnetic spectra considering various plausible scenarios and compare with the WA98 [2] photon and CERES/NA45 [3] dilepton spectra in order to comment on the relative importance of the two scenarios mentioned above.

Our analysis will proceed as follows. In the following section we will define the effective mass and width that have been used in the calculation and define the scenarios of medium effects considered. At the onset we emphasize that our main objective is to see the effect of these contrasting scenarios on the electromagnetic spectra and not on the details of how the forms of the effective mass and the width have been arrived at. Consequently, we will use phenomenological arguments to justify our choice of the parametrizations for these quantities. In Sec. III we will discuss the initial conditions in considerable detail. In the relevant transverse momentum region of the photon spectra the main sources of photons are the hard perturbative QCD processes as well as the thermal emissions. Consequently, the number of participants as well as the initial temperature are the relevant initial conditions that have been estimated. For the low mass dilepton spectra, the contribution from Dalitz decays as well as thermal emissions are important. Since photons and dileptons are emitted at all stages of the collision, the space-time evolution plays a very significant role in estimating the total yield. We have used two different approaches to study this aspect: relativistic hydrodynamics and transport. As we shall see, medium effects do play a very important role in the equation of state and consequently the cooling profile. These aspects have been dealt with in Sec. IV. The transverse mass (m_T) spectra of pions and protons obtained at SPS have been evaluated and compared with data from NA49 [4] in Sec. V in order to estimate the freeze-out condition that goes as an input into the hydrodynamic calculations. With all these inputs we evaluate the photon and dilepton spectra in Secs. VI and VII, respectively. Section VIII contains a summary and discussions.

II. EFFECTIVE MASS AND WIDTH OF HADRONS

It has been emphasized that the properties of hadrons will be modified due to their interaction with the particles in the thermal bath and such modifications will be reflected in the dilepton and photon spectra emitted from the system (see Refs. [5–9] for review). Broadly, two types of medium modifications are expected: shift in the pole position and/or broadening of the spectral function. As discussed earlier, our main objective is to comment on the nature of medium effects through the study of WA98 photon and CERES dilepton data. Accordingly, we consider the following scenarios.

(i) The system is formed in the hadronic phase with the hadronic masses (except pseudoscalars) approaching zero near the critical temperature according to the universal scaling law [5,10]. The in-medium masses of the hadrons and the decay width of ρ are taken as

$$m_H^*/m_H=(1-T^2/T_c^2)^{\lambda},$$

$$\Gamma_\rho=\frac{g_{\rho\pi\pi}^2}{48\pi}m_\rho^*(1-4m_\pi^2/m_\rho^{*2})^{3/2}(1+2f_{BE}), \qquad (1)$$

where $f_{BE}=(e^{\beta E}-1)^{-1}$ is the Bose-Einstein distribution. For the width of ω see Ref. [9].

(ii) The width of the vector meson (ρ) increases with temperature as

$$\Gamma_\rho^*=\Gamma_\rho/(1-T^2/T_c^2),$$

$$m_H^*=m_H \qquad (2)$$

and the masses remain constant at their vacuum values. The values of λ in Eq. (1) are 1/6 and 1/2 for Brown-Rho and Nambu scalings [5], respectively. The present experimental statistics cannot differentiate among different values of λ. Therefore, we leave it as a parameter here. The scenario (ii) derives motivation from the results of chiral models according to which the mass of the ρ does not change to order T^2, but the leading order T dependence of the pion decay constant results in the ρ decay width having the form described by Eq. (2). We have also considered a third case, (iii), in which both the masses and widths are maintained at the vacuum values. In Eqs. (1) and (2), T_c is the critical temperature of chiral symmetry restoration where the quark condensate $\langle\bar{q}q\rangle$ and consequently the mass of the hadrons tend to zero. In this work we assume $T_c\sim T_i$, which is the initial temperature of the system.

Let us study the in-medium effects on the thermal phase space factor through the ρ meson as it plays the most important role for the electromagnetic probes. The density of an unstable vector meson (ρ in this case) in a thermal bath can be written as [11]

$$\frac{dN}{d^3kd^3xds}=\frac{g}{(2\pi)^3}\frac{1}{e^{\sqrt{k^2+s}/T}-1}P(s), \qquad (3)$$

where g is the statistical degeneracy of the particle and $P(s)$ is the spectral function,

$$P(s)=\frac{1}{\pi}\frac{\mathrm{Im}\,\Pi}{(s-m_\rho^2-\mathrm{Re}\,\Pi)^2+(\mathrm{Im}\,\Pi)^2}. \qquad (4)$$

$\mathrm{Im}\,\Pi$ ($\mathrm{Re}\,\Pi$) is the imaginary (real) part of the ρ self-energy. Equations (3) and (4) indicate that the density of particles (vector mesons) in a thermal bath is given by the Bose-Einstein distribution weighted by the Breit-Wigner function, which gets maximum weight from the value of $s=m_\rho^2+\mathrm{Re}\,\Pi$, the contribution from either side of the maximum being averaged out. Therefore, the results become sensitive to the value of $s=m_\rho^{2*}=m_\rho^2+\mathrm{Re}\Pi$ and not to the width of the spectral distribution. Note that $P(s)$ tends to $\delta(s-m_\rho^2-\mathrm{Re}\Pi)$ as $\mathrm{Im}\,\Pi\to 0$, corresponding to a stable particle. (Here, Π is proportional to the trace of the self energy tensor $\Pi_{\mu\nu}$ of ρ.) In Fig. 1 we plot the density of thermal ρ mesons,

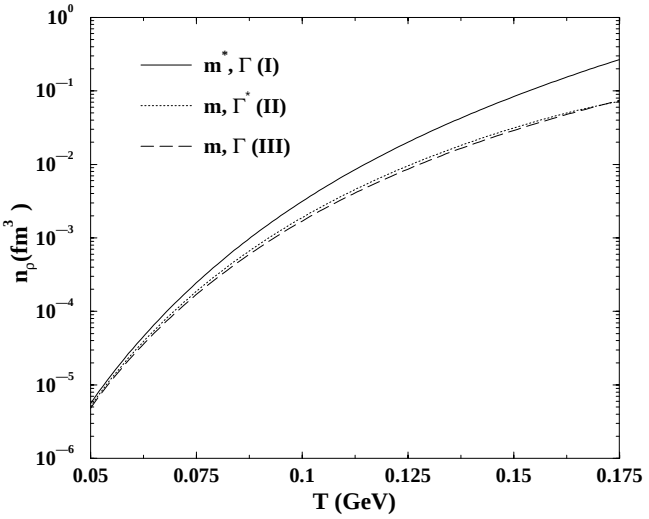

FIG. 1. Solid (long-dashed) line represents density of thermal ρ as a function of temperature with in-medium mass and vacuum width (vacuum mass and width). Dotted line represents the density with vacuum mass and in-medium width.

n_ρ, as a function of temperature [obtained by integrating Eq. (3) over d^3k and ds] for scenarios (i), (ii), and (iii). These are indicated by solid, dotted, and long-dashed lines, respectively. It is clear that the density of ρ is very sensitive to the spectral shift of ρ mass due to Boltzmann enhancement, but rather insensitive to the change of width as discussed above.

III. INITIAL CONDITIONS

Here we will discuss the parameters that enter as inputs to the evaluation of electromagnetic and hadronic spectra from relativistic heavy ion collisions corresponding to different scenarios considered. We begin with the quantity $n(b)$ which is the average number of nucleon-nucleon collisions in the collision of two nuclei of mass numbers A and B at an impact parameter b. This is given by [12]

$$n(b)=ABT_{AB}(b)\sigma_{in}, \qquad (5)$$

where σ_{in} (=30 mb, taken from Ref. [2]) is the p-p inelastic cross section and $T_{AB}(b)$ is the nuclear overlap integral evaluated from the following expression:

$$T_{AB}(\vec{b})=\int d^2sT_A(\vec{s})T_B(\vec{b}-\vec{s}), \qquad (6)$$

and the thickness function T_A is defined as $T_A(\vec{b})=\int dz\rho_A(\vec{b},z)$. The nuclear density $\rho_A(\vec{b},z)$ is parametrized by Woods-Saxon type profile function [13],

$$\rho_A(r)=\frac{\rho_0}{1+e^{(r-R_A)/z}}, \qquad (7)$$

where $z=0.549$ for the Pb nucleus, $R_A=1.2A^{1/3}$, and the central density ρ_0 is determined by the normalization condition $\int d^3r\rho_A(r)=1$. In Fig. 2 $n(b)$ is shown as a function of

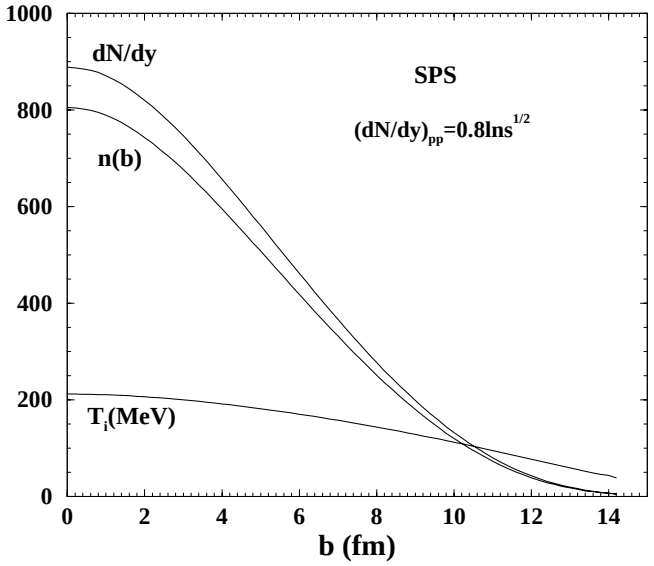

FIG. 2. The hadron multiplicity dN/dy, effective number of nucleon-nucleon collisions $n(b)$, and initial temperature T_i (in MeV) as a function of impact parameter b calculated by using Glauber model for nucleus-nucleus collisions (see text).

the impact parameter b. The most central event in WA98 corresponds to $b\sim 3.2$ fm/c. At this value of the impact parameter $n(b)\sim 660$.

The hadron multiplicity in $A+B$ collisions at an impact parameter b can then be evaluated in terms of the multiplicity in pp collisions as [12]

$$\frac{dN}{dy}(b)=\frac{n(b)}{1+\delta(A^{1/3}+B^{1/3})}\frac{dN_{pp}}{dy}, \tag{8}$$

where $dN_{pp}/dy=0.8\ln\sqrt{s}$ is the hadron multiplicity for nucleon-nucleon collisions at mid-rapidity [14]. The value of dN/dy is 725 at $b\sim 3.2$ fm, $\sqrt{s}=17.3$ GeV, and $\delta=0.09$ (see Ref. [12]). The term $1+\delta(A^{1/3}+B^{1/3})$ takes into account the energy degradation of the participating nucleons in the nuclear environment. For isentropic expansion the initial temperature (T_i) is related to the hadron multiplicity as

$$T_i^3(b)=\frac{2\pi^4}{45\xi(3)}\frac{1}{\pi R_A^2\tau_i 4a_k}\frac{dN}{dy}(b), \tag{9}$$

$a_k=\pi^2 g_k/90$ is determined by the statistical degeneracy (g_k) of the system formed after the collision. In case of a deconfined initial state $g_k=37$, considering a noninteracting gas of gluons and quarks of two flavors. For the hadronic gas we evaluate the entropy density by assuming the system to consist of free hadrons with effective mass m^* at a temperature T (see Ref. [9] for details). Then the effective degeneracy g_{eff} for the hadronic phase is obtained by the relation $s_H=4\,\pi^2 g_{eff}(m^*,T)T^3/90$. This type of parametrization indicates that the hadronic matter with finite (temperature dependent) mass of hadrons can be effectively visualized as a gas of massless hadrons with an effective degeneracy $g_{eff}(m^*,T)$. Such a simplification helps us to understand the lifetime of various phases, expansion rate of the system, etc., at least semiquantitatively (the fourth part of Ref. [1]). Because of the temperature dependence of g_{eff}, Eq. (9) becomes transcendental, which has been solved self-consistently (see Ref. [9] for details) to obtain T_i. For a hadron gas composed of π, ρ, ω, η, a_1, and nucleons the effective degeneracy has a value ~ 30 near the critical temperature where the hadronic masses go to zero according to the universal scaling scenario [5]. A value of $g_{eff}\sim 30$ can also be realized from the lattice data [15,16] near the phase transition point. For $\tau_i=1$ fm/c [17] and $g_k\sim 30$, we get an initial temperature $T_i(b\sim 3.2\ \text{fm})\sim 200$ MeV (see Fig. 2). Note that the variation of $T_i(b)$ as a function of the impact parameter is very slow because $T_i(b)\sim[dN/dy(b)]^{1/3}$. The value of T_i is ~ 246 MeV for both the scenario (ii) and (iii) for $dN/dy\sim 725$ and $\tau_i=1$ fm/c. This value of T_i appears to be too high for the hadrons to survive and we therefore exclude this possibility here.

IV. SPACE-TIME EVOLUTION AND EQUATION OF STATE

Next we study the sensitivity of the results on the space-time evolution. In order to do that we solve the (3+1) dimensional hydrodynamic equations with initial energy density [18],

$$\epsilon(\tau_i,r)=\frac{\epsilon_0}{e^{(r-R_A)/\delta}+1} \tag{10}$$

and initial radial velocity, $v_r(\tau_i,r)=0$.

The equation of state (EOS) used here to solve the hydrodynamic equations is evaluated as in Ref. [9]. The temperature dependence of the mass enters into the EOS through the effective statistical degeneracy (g_{eff}). In Fig. 3 the temperature variation of the effective degeneracy obtained from different models for the hadronic interactions (see Ref. [9] for details) is compared with the lattice QCD calculations [15]. The coefficient of ϵ/T^4 differs from the effective degeneracy by a factor of $\pi^2/30$. The lattice data seem to be well reproduced by the universal scaling scenario of mass reduction given by Eq. (1). Therefore, the increase of the effective statistical degeneracy near the critical point in lattice QCD calculations may be understood by assuming the heavier hadrons going to massless situation near T_c [19,20]. In this case the velocity of sound (c_s) is given by $c_s^{-2}=Tds/sdT=[(T/g_{eff})(dg_{eff}/dT)+3]$ [21]. Clearly, the value of c_s is less than its value corresponding to ideal fluid case ($c_s^{ideal}=1/\sqrt{3}$). This affects the space-time evolution of the system nontrivially. In solving the hydrodynamic equations we have used the equation of state that contains the in-medium shift of the hadronic spectral functions as described above.

The integration over the space-time history has also been performed by taking the temperature profile from the transport model where the temperature varies with time as follows:

$$T(t)=(T_i-T_\infty)e^{-t/\tau}+T_\infty. \tag{11}$$

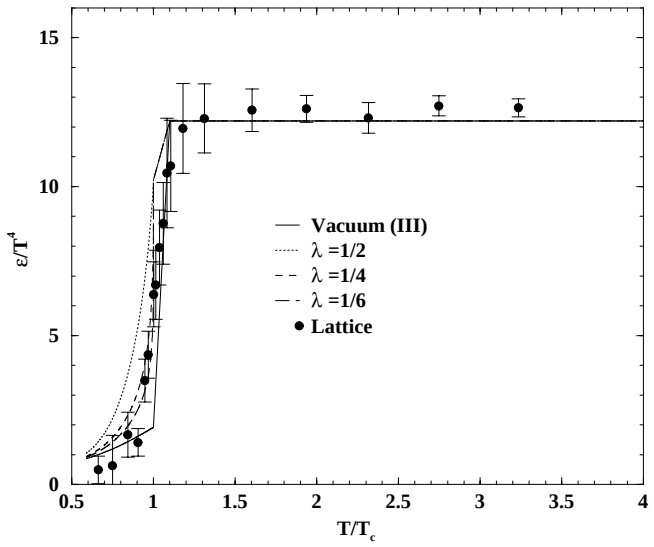

FIG. 3. The energy density ϵ in the unit of T^4 for the equation of state for various models of hadronic interactions is plotted as a function of temperature (T) in the unit of the critical temperature T_c. The filled circle denotes the lattice results [15]. The universal scaling scenario seems to describe the lattice results quite well near the T_c. For $T>T_c$ the bag model equation of state has been used.

The cooling law given above is the parametrization of the results of Ref. [22], used in several papers in the literature [23] (see also the review [8] and references therein). The calculation is performed with the following values of parameters: $T_i=200$ MeV, $T_\infty=120$ MeV, and $\tau=8$ fm/c.

V. HADRONIC SPECTRA AND FREEZE-OUT TEMPERATURE

Having fixed the initial temperature and the equation of state we now need to fix another important parameter, the freeze-out temperature T_F where the hydrodynamic evolution should terminate. At this stage the mean free path of the constituents begins to exceed the size of the system and particles start free streaming to the detector. For this purpose we will consider the $m_T(=\sqrt{p_T^2+m^2})$ spectra [24,25] of pions and protons measured in Pb+Pb collisions at SPS energies by the NA49 Collaboration [4]. We will assume that pions and nucleons are in thermal equilibrium throughout the evolution until they freeze-out at a common temperature T_F. Negative hadrons and positive minus the negative are treated as pions and protons, respectively. The π^- and K^- from the decays ρ and ϕ are about 5% of the direct pions at $p_T\sim 500$ MeV and are therefore neglected here. In Fig. 4, NA49 pion spectra are compared with the hadronic initial states with $T_i\sim 200$ MeV and $T_F=$ 100, 120, and 140 MeV. We find a reasonable agreement for $T_F=120$ MeV as far as the slope is concerned. Calculations are done with all the scenarios (i), (ii), and (iii). Due to reasons explained in Sec. II, the results with scenario (ii) are indistinguishable from that of scenario (iii). We arrive at similar conclusions from the analysis of the proton spectra as shown in Fig. 5.

It should be pointed out that there is no unique description

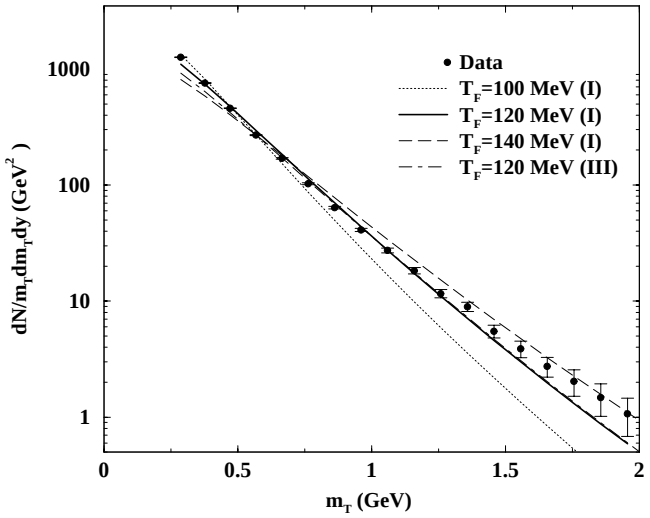

FIG. 4. The m_T distribution of pions for Pb+Pb collisions at CERN SPS energies.

so far for the p_T spectra of hadrons. It has been shown in Ref. [26] that the WA80 and WA98 π^0 spectra can be reproduced by perturbative QCD calculation if the initial p_T broadening is taken into account. Wang [26] has claimed that the transverse mass spectra of π^0 in central Pb+Pb collisions cannot be due to collective flow. The p_T broadening in heavy ion collisions can also be explained reasonably well by a random walk model [27] where transverse flow effects are not required to reproduce the data. It has been suggested recently that the p_T broadening in high energy nuclear collisions can be generated by the color glass condensate, i.e., by the initial partonic phase formed after the collisions [28]. Keeping these possible scenarios in mind we do not attempt to reproduce the absolute normalization of the m_T spectra of the pions by hydrodynamic flow. We rather concentrate on the effects of the EOS containing the in-medium mass modification of hadrons on the m_T spectra of pions and protons.

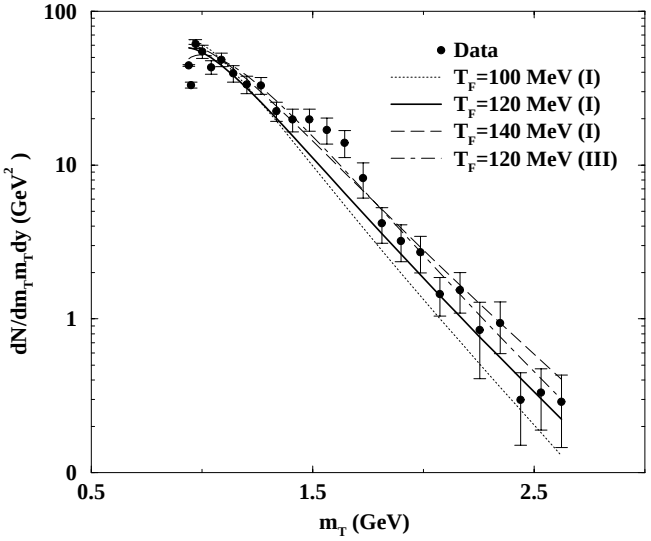

FIG. 5. The m_T distribution of protons for Pb+Pb collisions at CERN SPS energies.

The normalizations of pions and nucleons are treated as parameters to be determined by the experimentally measured spectra (for the details of the theoretical calculations see Refs. [29,24,25]).

VI. PHOTON SPECTRA

We start with the single photon data of the WA98 Collaboration that has initiated considerable theoretical activities [30–35]. For the analysis of WA98 photon spectra, we consider prompt photons resulting from the hard collisions of the partons in the colliding nuclei and the thermal photons from a hot hadronic gas with possible in-medium modifications. Photons from hadronic decays ($\pi^0 \to \gamma\gamma$, $\eta \to \gamma\gamma$, etc.) are already subtracted from the data [2] and hence we need not consider them here. We begin our discussions with the prompt photon. The prompt photon yield for nucleus-nucleus collision is given by

$$E\frac{dN}{d^3p} = n(b)\frac{1}{\sigma_{in}} E\frac{d\sigma_{pp}}{d^3p}, \tag{12}$$

where $n(b)$ is the average number of nucleon-nucleon collisions at an impact parameter b. The prompt photon contributions have been evaluated with possible intrinsic transverse motion of the partons [34,36] inside the nucleon and multiplied by a K factor ~ 2, to account for the higher order effects. The CTEQ(5M) parton distributions [37] have been used for evaluating hard photons. The relevant value of $\sqrt{s}$, energy in the center of mass, for WA98 experiment is 17.3 GeV. No experimental data on hard photons exist at this energy. Therefore, the "data" at $\sqrt{s}=17.3$ GeV are obtained from the data at $\sqrt{s}=19.4$ GeV of the E704 Collaboration [38] by using the scaling relation: $Ed\sigma/d^3p_\gamma|_{h_1+h_2\to C+\gamma} = f(x_T = 2p_T/\sqrt{s})/s^2$, for the hadronic process $h_1+h_2 \to C+\gamma$ [39]. This scaling is valid in the naive parton model. However, such scaling may be spoiled in perturbative QCD due to the reasons, among others, the momentum dependence of the strong coupling, α_s and from the scaling violation of structure functions, resulting in faster decrease of the cross section than $1/s^2$ [36]. Therefore, the data at $\sqrt{s}=17.3$ GeV obtained by using the above scaling give a conservative estimate of the prompt photon contributions. We have seen that the effects of the nuclear shadowing in parton distributions on the prompt photons are negligibly small at SPS but are important at Relativistic Heavy Ion Collider (RHIC) and LHC energies [40]. This is because the value of $x(\sim 2p_T/\sqrt{s})$ at SPS is not small enough for the shadowing effects to be important.

To evaluate the photon emission rate from a hadronic gas we model the system as consisting of π, ρ, ω, η, and a_1 [41,42]. The relevant vertices for the reactions $\pi\pi \to \rho\gamma$ and $\pi\rho \to \pi\gamma$ and the decay $\rho \to \pi\pi\gamma$ are obtained from the following Lagrangian:

$$\mathcal{L} = -g_{\rho\pi\pi}\vec{\rho}^{\mu}(\vec{\pi}\times\partial_\mu\vec{\pi}) - eJ^\mu A_\mu + \frac{e}{2}F^{\mu\nu}(\vec{\rho}_\mu\times\vec{\rho}_\nu)_3, \tag{13}$$

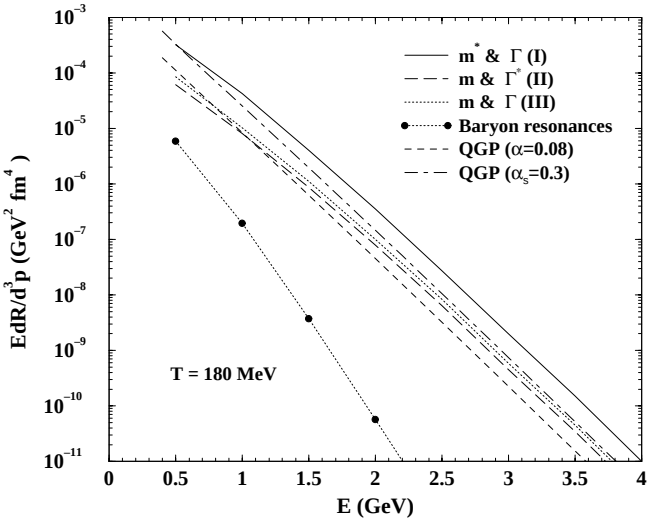

FIG. 6. The photon production rate as a function of its energy at a temperature $T=180$ MeV. Solid (long-dashed) line indicates rate for scenario (i) [scenario (ii)]. Dotted line represents the spectra without any medium effects (scenario (iii)). Filled circles indicate photons originating from baryonic resonance decays. Short-dashed (dot-dashed) line indicates the photon emission rate from a thermalized two-flavor quark gluon plasma for $\alpha_s = 0.08(0.2)$.

where $F_{\mu\nu} = \partial_\mu A_\nu - \partial_\nu A_\mu$ is the field tensor for electromagnetic field and J^μ is the hadronic part of the electromagnetic current given by

$$J^\mu = (\vec{\rho}_\nu \times \vec{\varrho}^{\nu\mu})_3 + [\vec{\pi}\times(\partial^\mu\vec{\pi} + g_{\rho\pi\pi}\vec{\pi}\times\vec{\rho}^{\mu})]_3, \tag{14}$$

with $\vec{\varrho}_{\mu\nu} = \partial_\mu\vec{\rho}_\nu - \partial_\nu\vec{\rho}_\mu - g_{\rho\pi\pi}(\vec{\rho}_\mu\times\vec{\rho}_\nu)$. $\vec{\pi}$, $\vec{\rho}^\mu$, and A^μ represent the π, ρ, and photon fields, respectively, and the arrows represent vectors in isospin space. $g_{\rho\pi\pi}$ denotes the coupling strength of the $\rho\pi\pi$ vertex, fixed from the observed decay width $\rho \to \pi\pi$. We have also considered the photon production due to the reactions $\pi\eta \to \pi\gamma$, $\pi\pi \to \eta\gamma$, and the decay $\omega \to \pi\gamma$ using the interaction given in Ref. [43] and vector meson dominance [44]:

$$\mathcal{L} = \frac{g_{\rho\rho\eta}}{m_\eta}\epsilon_{\mu\nu\alpha\beta}\partial^\mu\rho^\nu\partial^\alpha\rho^\beta\eta + \frac{g_{\omega\rho\pi}}{m_\pi}\epsilon_{\mu\nu\alpha\beta}\partial^\mu\omega^\nu\partial^\alpha\rho^\beta\pi + \sum_{V=\rho,\omega}\frac{em_V^2}{g_V}V^\mu A_\mu, \tag{15}$$

where $\epsilon_{\mu\nu\alpha\beta}$ is the totally antisymmetric Levi-Civita tensor. The invariant amplitudes for all the reactions are given in Ref. [42]. The values of $g_{\rho\rho\eta}$ and $g_{\omega\rho\pi}$ are fixed from the observed decays, $\rho \to \eta\gamma$ and $\omega \to \pi\gamma$, respectively. The constant g_V is determined from the decays, $V \to e^+e^-$. Photon production due to the process $\pi\rho \to a_1 \to \pi\gamma$ is also taken into consideration (for details of interaction vertices see Ref. [9]).

In Fig. 6 the static (fixed temperature) photon spectra are shown for $T=180$ MeV. The solid line shows the enhanced yield with in-medium masses and vacuum widths compared to the yield obtained with vacuum masses and widths (dotted

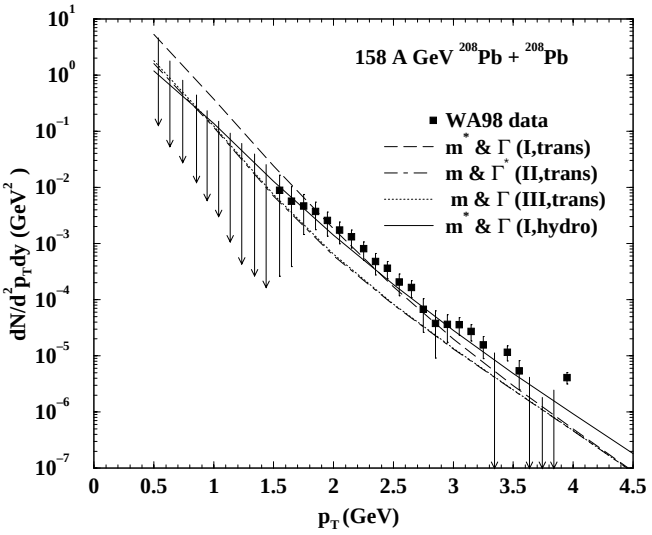

FIG. 7. Total (prompt+thermal) photon yield in Pb+Pb collisions at 158*A* GeV at CERN-SPS. The theoretical calculations contain hard QCD and thermal photons. The system is formed in the hadronic phase with initial temperature $T_i=200$ MeV; "trans" indicates the results for cooling law (11).

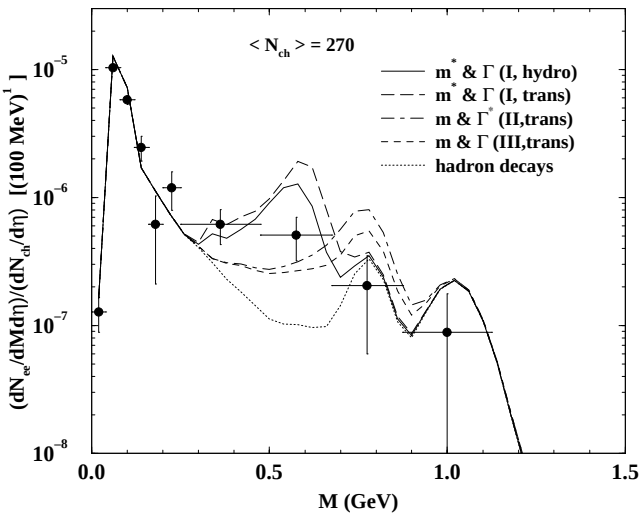

FIG. 8. Dilepton spectra for $\langle N_{ch}\rangle=270$ for different scenarios as indicated in the text.

line). The long-dashed line showing the result with in-medium width and vacuum masses does not differ substantially from the dotted line, because we find that the effects of the change in the decay width, both on the phase space and the production cross section, are small. We observe that the contributions from the decays of baryonic resonances [$N(1520)$, $N(1535)$, $N(1440)$, $\Delta(1232)$, and $\Delta(1620)$] are also small (filled circle). The values of the decay widths, $R \rightarrow N\,\gamma$, where R and N denote the baryonic resonances and the nucleon, respectively, are taken from Ref. [45]. It is observed that the photon yield with universal mass variation scenario (i) is almost an order magnitude larger than case (ii) with large broadening of ρ. Reduction in the hadronic masses causes an enhancement in the thermal distribution of mesons because of which the rate of thermal emission of photons increases. The scenario with vacuum values of both masses and width (dotted line) does not show any appreciable difference from (ii).

For the sake of comparison we have also shown the photon emission rate from a thermalized QGP. The photon spectra from QGP include Compton, annihilation, bremsstrahlung, and annihilation with scattering processes [41,46–48] (see also Ref. [49]). Here we have mainly focused on photon production from hot hadronic matter and hence do not consider emission rate from QGP beyond two loops [50].

In Fig. 7 the p_T distribution of photons (prompt+thermal) is compared with the WA98 data. Within the framework of the transport model the data are well reproduced when the hadronic masses are allowed to vary according to Eqs. (1) [long-dash line, scenario (i)]. However, when scenario (ii) is considered for thermal photons (dash-dotted line) the experimentally observed "excess" photon in the region $1.5 \leqslant p_T$ (GeV) $\leqslant 2.5$ is not reproduced. The dotted line indicates results with vacuum masses and widths.

The photon yield for scenario (i) shown in Fig. 7 (solid line) is obtained by folding the static rate with the space-time history of the system governed by relativistic hydrodynamics from the initial to the freeze-out state (freeze-out temperature $\sim$120 MeV); the data are well reproduced in this case also.

The agreement between the p_T spectra of photon obtained with two different types of space-time evolution scenarios (transport model and hydrodynamics) can be explained as follows. We find that the variation of temperature with time (cooling law) in Eq. (11) is slower than the one obtained by solving hydrodynamic equations. As a consequence, the thermal system has a longer lifetime than the former case, allowing the system to emit photons for a longer time. In case of hydrodynamics this is compensated by the transverse kick due to radial velocity of the expanding matter, which shifts some of the photon multiplicity from lower values of transverse momentum towards the higher region.

VII. DILEPTON SPECTRA

Now we study the invariant mass distribution of lepton pairs measured by the CERES/NA45 Collaboration [3] in Pb+Au collisions. We consider the thermal dilepton production in the hadronic medium due to the process $\pi^+\pi^- \rightarrow e^+e^-$, known to be the most dominant source of dilepton production from hadronic matter. In the thermal system the width of the ω meson can be large due to various reactions occurring in the thermal bath, the most dominant process, among others, is $\omega\pi \leftrightarrow \pi\pi$ [9,51]. As a consequence of this, the lifetime of the ω meson could become smaller compared to the lifetime of the hadronic system, enabling it to decay in the interior of the system. In view of this, the in-medium decay $\omega \rightarrow e^+e^-$ is also taken into account. The required interaction vertices have been obtained from Eqs. (13), (14), and (15). In Fig. 8 the experimental data are compared with the theoretical results for $dN_{ch}/d\eta=270$. The effective masses and widths of ρ and ω mesons appearing in the processes $\pi\pi \rightarrow \rho \rightarrow e^+e^-$ and $\omega \rightarrow e^+e^-$, respectively, are taken from Eq. (1) (for details on the the thermal emission rate of lepton pairs see Ref. [9]). Contributions from had-

ronic decays at freeze-out (background) are taken from the second part of Ref. [3] (dotted line). The observed enhancement of the dilepton yield around $M \sim 0.3$–0.6 GeV can be reproduced by scenarios (i) (long-dashed line) and (ii) (dot-dashed line) when the cooling law is taken as Eq. (11). The data are also well reproduced when hydrodynamics is used to describe the space-time evolution of system for scenario (i) (solid line). However, with vacuum properties of the vector mesons the low mass enhancement cannot be reproduced (short-dashed line), indicating the change of vector meson properties in the medium. It is interesting to recall here that in a recent experiment Ozawa *et al.* [52] has observed a significant enhancement in the dilepton yield in p + Cu collisions as compared to $p+\mathrm{C}$ collisions below the ω peak.

VIII. SUMMARY AND DISCUSSIONS

Let us now summarize the results. We reiterate that our main contention in this work is to comment on the nature of medium effects vis-à-vis mass shift as opposed to broadening of the spectral density of hadrons. Such a study is only possible through the electromagnetic probes since they are sensitive to the evolution of the spectral function of vector mesons. The freeze-out conditions within the model used for evaluating the photon and dilepton spectra have been estimated through the NA49 pion and proton spectra. First, we find that the WA98 photon transverse momentum spectra and the CERES dilepton low invariant mass spectra are well explained if we assume a chirally restored initial phase at a temperature ~ 200 MeV where the masses of the hadrons tend to zero and grow to their vacuum values with the decrease of temperature. In fact, close to the critical temperature for chiral symmetry restoration (in our case $\sim T_i = 200$ MeV) the description of the system either in terms of partonic or hadronic degrees of freedom become dual, although the nonperturbative effects may still be important. For example, the emission rate of dileptons from pion annihilation will resemble that from $q\bar{q}$ annihilation, because of the complete extinction of the intermediary ρ at the critical temperature [8,9]. This indicates that the $q\bar{q}$ interaction in the vector channel has become weak, signaling the onset of chiral transition. Whether such a state is synonymous with deconfined matter (QGP) is still an unsettled issue. A similar value of the initial temperature is obtained in Refs. [31,32,21,53]. Based on the present and our earlier results [31], it is fair to say that a simple hadronic model with vacuum properties of hadrons is inadequate to explain the above experimental data. Either a substantial change in the in-medium hadronic spectral function or the formation of the QGP is required. More importantly, we find that the p_T distribution of photons changes significantly with a reduced mass scenario and is almost unaffected by the broadening of the vector meson spectral function in the medium. The invariant mass distribution of the lepton pairs, on the other hand, can be explained with both a reduction in the mass as well as with an enhanced width of the vector mesons. Thus by looking only at the dilepton spectra it is difficult to differentiate the above scenarios; we need to analyze both the photon and dilepton spectra simultaneously. With better statistics we might succeed in ruling out or at least restricting one of the scenarios. We expect that such a situation should be realized at RHIC.

ACKNOWLEDGMENTS

We are grateful to Tetsuo Hatsuda for useful comments on this manuscript. Useful discussions with Tapan K. Nayak are thankfully acknowledged. J.A. is grateful to the Japan Society for Promotion of Science (JSPS) for financial support. J.A. is also supported by a Grant-in-aid for Scientific Research No. 98360 of JSPS.

[1] L. McLerran and T. Toimela, Phys. Rev. D **31**, 545 (1985); C. Gale and J.I. Kapusta, Nucl. Phys. **B357**, 65 (1991); E.V. Shuryak, Phys. Rep. **61**, 71 (1980); J. Alam, S. Raha, and B. Sinha, *ibid.* **273**, 243 (1996); W. Cassing and E.L. Bratkovskaya, *ibid.* **308**, 65 (1999).
[2] M.M. Aggarwal *et al.*, WA98 Collaboration, Phys. Rev. Lett. **85**, 3595 (2000).
[3] G. Agakichiev *et al.*, CERES Collaboration, Phys. Lett. B **422**, 405 (1998); B. Lenkeit, doctoral thesis, Universitaet Heidelberg, 1998.
[4] H. Appelshäuser *et al.*, NA49 Collaboration, Phys. Rev. Lett. **82**, 2471 (1999).
[5] G.E. Brown and M. Rho, Phys. Rep. **269**, 333 (1996); **363**, 85 (2002).
[6] T. Hatsuda and T. Kunihiro, Phys. Rep. **247**, 221 (1994).
[7] R.D. Pisarski, hep-ph/9503330.
[8] R. Rapp and J. Wambach, Adv. Nucl. Phys. **25**, 1 (2000).
[9] J. Alam, S. Sarkar, P. Roy, T. Hatsuda, and B. Sinha, Ann. Phys. (N.Y.) **286**, 159 (2000).
[10] G.E. Brown and M. Rho, Phys. Rev. Lett. **66**, 2720 (1991).
[11] H.A. Weldon, Ann. Phys. (N.Y.) **228**, 43 (1993).
[12] C. Y. Wong, *Introduction to High Energy Heavy Ion Collisions* (World Scientific, Singapore, 1994).
[13] K.J. Eskola, R. Vogt, and X.N. Wang, Int. J. Mod. Phys. A **10**, 3087 (1995).
[14] U. Heinz, P. Koch, and B. Friman, in Proceedings of Large Hadron Collider Workshop, Aachen, 1990, edited by G. Jarlskog and D. Rein, Vol. II, p. 1079.
[15] F. Karsch, Nucl. Phys. **A698**, 199 (2002).
[16] M. Asakawa and T. Hatsuda, Phys. Rev. D **55**, 4488 (1997).
[17] J.D. Bjorken, Phys. Rev. D **27**, 140 (1983).
[18] H. von Gersdorff, M. Kataja, L. McLerran, and P.V. Ruuskanen, Phys. Rev. D **34**, 794 (1986).
[19] V. Koch and G.E. Brown, Nucl. Phys. **A560**, 345 (1993).
[20] G.E. Brown, H.A. Bethe, A.D. Jackson, and P.M. Pizzochero, Nucl. Phys. **A560**, 1035 (1993).
[21] S. Sarkar, J. Alam, and T. Hatsuda, nucl-th/0011032.
[22] G.Q. Li, C.M. Ko, and G.E. Brown, Phys. Rev. Lett. **75**, 4007 (1995); Nucl. Phys. **A606**, 568 (1996).
[23] R. Rapp, G. Chanfray, and J. Wambach, Phys. Rev. Lett. **76**,

368 (1996); Nucl. Phys. **A617**, 472 (1997).
[24] P.V. Ruuskanen, Acta Phys. Pol. A **18**, 551 (1986).
[25] J. P. Blaizot and J. Y. Ollitrault, in *Quark Gluon Plasma*, edited by R.C. Hwa (World Scientific, Singapore 1992).
[26] X.N. Wang, Phys. Rev. Lett. **81**, 2655 (1998).
[27] A. Leonidov, M. Nardi, and H. Satz, Z. Phys. C **74**, 535 (1997); J. Alam, J. Cleymans, K. Redlich, and H. Satz, nucl-th/9707042.
[28] L. McLerran and J. Schaffner-Bielich, Phys. Lett. B **514**, 29 (2001); J. Schaffner-Bielich, D. Kharzeev, L. McLerran, and R. Venugopalan, Nucl. Phys. **A705**, 494 (2002).
[29] U. Heinz, K. S. Lee, and E. Schnedermann, in *Quark Gluon Plasma*, Ref. [25].
[30] K. Gallmeister, B. Kämpfer, and O.P. Pavlenko, Phys. Rev. C **62**, 057901 (2000).
[31] J. Alam, S. Sarkar, T. Hatsuda, T.K. Nayak, and B. Sinha, Phys. Rev. C **63**, 021901(R) (2001).
[32] D.Yu. Peressounko and Yu.E. Pokrovsky, hep-ph/0009025.
[33] S. Sarkar, P. Roy, J. Alam, and B. Sinha, Phys. Rev. C **60**, 054907 (1999).
[34] C.Y. Wong and H. Wang, Phys. Rev. C **58**, 376 (1998).
[35] D.K. Srivastava and B. Sinha, Phys. Rev. C **64**, 034902 (2001).
[36] J.F. Owens, Rev. Mod. Phys. **59**, 465 (1987).
[37] H.L. Lai *et al.*, Eur. Phys. J. C **12**, 375 (2000).
[38] D.L. Adams *et al.*, E704 Collaboration, Phys. Lett. B **345**, 569 (1995).
[39] T. Ferbel and W.R. Molzon, Rev. Mod. Phys. **56**, 181 (1984).
[40] P. Roy *et al.* (unpublished).
[41] J.I. Kapusta, P. Lichard, and D. Seibert, Phys. Rev. D **44**, 2774 (1991).
[42] S. Sarkar, J. Alam, P. Roy, A.K. Dutt-Mazumder, B. Dutta-Roy, and B. Sinha, Nucl. Phys. **A634**, 206 (1998); P. Roy, S. Sarkar, J. Alam, and B. Sinha, *ibid.* **A653**, 277 (1999).
[43] M. Gell-Mann, D. Sharp, and W.D. Wagner, Phys. Rev. Lett. **8**, 261 (1962).
[44] J. J. Sakurai, *Currents and Mesons* (The University of Chicago Press, Chicago, 1969).
[45] Particle Data Group, R.M. Barnett *et al.*, Phys. Rev. D **54**, 1 (1996).
[46] R. Baier, H. Nakkagawa, A. Niégawa, and K. Redlich, Z. Phys. C **53**, 433 (1992).
[47] P. Aurenche, F. Gelis, H. Zaraket, and R. Kobes, Phys. Rev. D **58**, 085003 (1998).
[48] F.D. Steffen and M.H. Thoma, Phys. Lett. **510**, 98 (2001).
[49] D. Dutta, S.V.S. Sastry, A.K. Mohanty, K. Kumar, and R.K. Choudhury, Nucl. Phys. **A710**, 415 (2002).
[50] The thermal photon emission rate from QGP complete to order α_s has recently been obtained in Ref. [54], which was used by Huovinen *et al.* [55] to analyze the WA98 photon data.
[51] J. Alam, S. Sarkar, P. Roy, B. Dutta-Roy, and B. Sinha, Phys. Rev. C **59**, 905 (1999).
[52] K. Ozawa *et al.*, Phys. Rev. Lett. **86**, 5019 (2001).
[53] R. Rapp and E. Shuryak, Phys. Lett. B **473**, 13 (2000); K. Gallmeister, B. Kämpfer, and O.P. Pavlenko, *ibid.* **473**, 20 (2000).
[54] P. Arnold, G.D. Moore, and L.G. Yaffe, J. High Energy Phys. **0111**, 057 (2001).
[55] P. Huovinen, P.V. Ruuskanen, and S.S. Rasanen, Phys. Lett. B **535**, 109 (2002).